Effect of Phosphate Precursor and Organic Additives on the Structural and Catalytic Properties of Amorphous Mesoporous $AlPO_4$ Materials

J. M. Campelo,* M. Jaraba, D. Luna, R. Luque, J. M. Marinas, and A. A. Romero

Departamento de Química Orgánica, Universidad de Córdoba, Campus de Rabanales, Edificio Marie Curie, Carretera Nacional IV-A, Km. 396, E-14014 Córdoba, Spain

J. A. Navio and M. Macias

Instituto de Ciencia de Materiales de Sevilla, Centro de Investigaciones Científicas "Isla de la Cartuja", Avda. Américo Vespucio, s/n, E-41092 Sevilla, Spain

Received February 4, 2003. Revised Manuscript Received June 12, 2003

Amorphous mesoporous $AlPO_4$ materials were prepared by a gel precipitation method using different phosphate precursors [H_3PO_4, $(NH_4)H_2PO_4$, and $(NH_4)_2HPO_4$], both in the presence and absence of an aluminum-complexing assisted gel agent (1,2-ethanediol, 1,2- and 1,3-propanediol, and 2-methyl-2,4-pentanediol), followed by calcination in the 773−1273 K range. TG/DTA, XRD, and laser-Raman spectroscopy showed that the method assisted by an organic additive resulted in $AlPO_4$ with higher thermal stabilities (crystallization was delayed), as well as high surface areas and pore volumes even after calcination at 1073/1273 K. In all cases, ^{27}Al and ^{31}P MAS NMR spectroscopy only indicated the formation of tetrahedral $Al(OP)_4$ and $P(OAl)_4$ units. Moreover, surface areas and pore volumes depended on the organic additive used. Thus, the $AlPO_4$ obtained in the presence of 1,3-propanediol and 2-methyl-2,4-pentanediol possessed higher thermal stabilities that resulted in larger surface areas and pore volumes. Surface acidity measurements, through chemisorption (measured by gas-chromatography) of pyridine and 2,6-dimethylpyridine at 473−573 K, indicated that the $AlPO_4$ obtained in the presence of 1,3-propanediol and 2-methyl-2,4-pentanediol exhibited surface acid sites even after calcination at 1273 K. Cyclohexene skeletal isomerization, which is a model reaction catalyzed by relatively strong acid sites, was also studied for further characterization of acidic properties. Good correlations between catalytic performance and acidic properties were found.

Introduction

It is well-known that amorphous aluminum orthophosphates are solid bifunctional acid−bases that can be used as catalysts and supports. As catalysts, they are active in several chemical processes (both in the gas phase and in the field of selective synthetic chemistry), such as isomerization, cracking, dehydration, alkylation, retroaldolization, oxidative dehydrogenation, rearrangement, nucleophilic substitution, cetalization, condensation, Diels−Alder cycloaddition, and decomposition of fluoro- and chlorofluorocarbons.[1−10] Aluminum orthophosphates were also used as supports for polymerization, oxidation, hydrogenation, condensation, reductive cleavage, or hydration catalysts.[2,11−13] Moreover, their texture, structure, and acid−base character as well as their catalytic properties are all dependent on a number of variables such as aluminum starting salt, P/Al ratio, precipitation medium, thermal treatment during drying and calcination, addition of alkali, fluoride, and sulfate ions,[2] and addition of a metal oxide[2,4,14−20] or a metal phosphate.[5,10,21,22] In the latter cases, the performance

* To whom correspondence should be addressed. Phone: +34-957-218-622. Fax: +34-957-212-066. E-mail: qo1capej@uco.es.

(1) Moffat, J. B. *Catal. Rev. Sci. Eng.* **1978**, *18*, 199.
(2) Bautista, F. M.; Campelo, J. M.; Garcia, A.; Luna, D.; Marinas, J. M.; Moreno, M. C.; Romero, A. A.; Navio, A. A.; Macias, M. *J. Catal.* **1998**, *173*, 333, and references therein.
(3) Aramendia, M. A.; Borau, V.; Jiménez, C.; Marinas, J. M.; Romero, F. J.; Urbano, F. J. *J. Mol. Catal. A* **2002**, *182−183*, 35.
(4) Mohamed, F. S.; Kiwan, H. H.; Mostafa, M. R. *Ads. Sci. Technol.* **2002**, *20*, 131.
(5) Takita, Y.; Ninomiya, M.; Miyake, H.; Wakamatsu, H.; Yoshinaga, Y.; Ishihara, T. *Phys. Chem. Chem. Phys.* **1999**, *1*, 4501.
(6) Takita, Y.; Wakamatsu, H.; Tokumaru, M.; Nishiguchi, H.; Ito, M.; Ishihara, T. *Appl. Catal. A* **2000**, *194−195*, 55.
(7) Dume, C.; Kervennal, J.; Hub, S.; Holderich, W. F. *Appl. Catal. A* **1999**, *180*, 421.
(8) Climent, M. J.; Corma, A.; Garcia, H.; Guil-Lopez, R.; Iborra, S.; Fornes, V. *J. Catal.* **2001**, *197*, 385.
(9) Climent, M. J.; Corma, A.; Iborra, S.; Velty, A. *J. Mol. Catal. A* **2002**, *182−183*, 327.
(10) Hutchings, G. J.; Hudson, I. D.; Bethell, D.; Timms, D. G. *J. Catal.* **1999**, *188*, 291.
(11) Fougret, C. M.; Holderich, W. F. *Appl. Catal. A* **2001**, *207*, 295.
(12) Bautista, F. M.; Campelo, J. M.; Garcia, A.; Luna, D.; Marinas, J. M.; Romero, A. A. *J. Chem. Soc., Perkin Trans. 2* **2002**, 227.
(13) Bautista, F. M.; Campelo, J. M.; Garcia, A.; Luna, D.; Marinas, J. M.; Romero, A. A. *Stud. Surf. Sci. Catal.* **2001**, *138*, 213.
(14) Ahmed, F. S.; Mostafa, M. R.; Kiwan, H. H. *Ads. Sci. Technol.* **2000**, *18*, 709.
(15) Bautista, F. M.; Campelo, J. M.; Garcia, A.; Luna, D.; Marinas, J. M.; Moreno, M. C.; Romero, A. A. *Appl. Catal. A* **1998**, *170*, 159.
(16) Bautista, F. M.; Campelo, J. M.; Garcia, A.; Luna, D.; Marinas, J. M.; Romero, A. A.; Colon, G.; Navio, A. A.; Macias, M. *J. Catal.* **1998**, *179*, 483.

10.1021/cm030206+ CCC: $25.00
Published on Web 07/19/2003

of such catalysts is greatly dependent on the nature of the metal oxide (Al_2O_3, B_2O_3, CsO, SiO_2, TiO_2, ZrO_2, ZnO, V_2O_5, MoO_3, or WO_3) or the metal phosphate (BPO_4, $CrPO_4$, vanadyl phosphate, etc.), the $AlPO_4$/metal oxide (or metal phosphate) ratio, preparation methods, and operating conditions. Furthermore, $AlPO_4$ are also used as supports for the covalent immobilization of enzymes.[23, 24]

Moreover, new catalysts or catalyst supports, with improved structural properties and porosities, are needed for many chemical synthesis reactions due to the important role played by the support in heterogeneous catalytic system performance. This is because the activity and stability of the catalyst in many cases are known to depend not only on the inherent catalytic properties of the active phase but also on the textural and physicochemical characteristics of the support as well. Furthermore, some cases showed pore size characteristics to be more significant than the chemical nature of the support. Therefore, the control of these support properties is an important issue. At the same time, oxides and mixed oxides stand out as the support materials for various catalytic applications. The sol−gel process[25,26] offers the unique advantage of the synthesis of binary mixed oxides with a homogeneous distribution of components. Textural properties of such oxides and mixed oxides are strongly dependent upon synthesis conditions. Recently, there has also been extensive research on the influence of an organic additive presence (able to interact with metal ions such as aluminum, zirconium, or titanium) in the synthesis medium, and on the structural, textural, and surface properties of oxides[27−34] and mixed oxides,[35−45] as well as on their catalytic performance for several reactions, such as isomerization,[41] alkylation,[27,36] oxidation,[30] alcohol conversion[38,42] or cumene cracking.[40] Thus, there are reports in the literature on the use of different organic additives to alter the structural properties and porosity of the sol−gel oxidic materials in order to prepare oxides or mixed oxides with specific properties. These additives include ketones, diketones, diols, carboxylic acids, esters, dihydroxylated carboxylic acids, and polymers [poly(ethylene glycol), poly(ethylene oxide), polyacrylamide] among other additives. The complexing/modifying organic agent added during the sol−gel synthesis results in different organic−inorganic interactions in the structure formation process. These interactions change the hydrolysis rate, the distribution of species formed by the initial monomer condensation, the hydrous gel structure, and, consequently, the dehydration process, thus producing radical changes in the pore structure of the final oxide material. In mixed oxides, the organic agent also allows control of the hydrolysis rate in the more active alkoxide precursor, resulting in a more homogeneous distribution of components and a more precise control of structural and pore properties. The textural properties of the materials thus obtained depend on the metal ratio, as well as the type, amount, and molecular weight of additive used in the preparation, and method of additive incorporation.

In this paper we report on the preparation of amorphous aluminum orthophosphate ($AlPO_4$) by a gel precipitation method using different phosphate precursors [H_3PO_4, $(NH_4)H_2PO_4$, and $(NH_4)_2HPO_4$], aluminum chloride, and aqueous ammonia. We also study the preparation of $AlPO_4$ catalysts by a complexing-agent-assisted gel ammonia precipitation method using H_3PO_4 (a precursor that leads to materials with higher pore volumes and pore diameters) and $AlCl_3 \cdot 6H_2O$, in the presence of several water-soluble dihydroxylated organic compounds (1,2-ethanediol, 1,2- and 1,3-propanediol, and 2-methyl-2,4-pentanediol) that are able to interact with aluminum ions. The method developed is based on the idea that the presence of these compounds could prevent $AlPO_4$ particle coarsening and mesopore collapse. The materials are characterized by several physical methods (TGA/DTA, XRD, Raman, SEM-EPMA, XPS, DRIFT, ^1H, ^{27}Al, and ^{31}P MAS NMR, and N_2 adsorption) emphasizing crystallization, phase structure, surface area, pore volume, and size distribution. Pyridine (PY) and 2,6-dimethylpyridine (DMPY) adsorption (473−573 K) as well as cyclohexene skeletal isomerization (CSI) into 1- and 3-methylcyclopentene, which is a model reaction catalyzed by relatively strong acid sites, were also studied for further characterization of their acidic properties. The results indicate that the

(17) Bautista, F. M.; Campelo, J. M.; Garcia, A.; Leon, R. M.; Luna, D.; Marinas, J. M.; Romero, A. A.; Navio, A. A.; Macias, M. *J. Mater. Chem.* **1999**, *9*, 827.
(18) Bautista, F. M.; Campelo, J. M.; Garcia, A.; Leon, R. M.; Luna, D.; Marinas, J. M.; Romero, A. A. *Catal. Lett.* **1999**, *60*, 145.
(19) Parida, K. M.; Acharya, M.; Mishra, T. *J. Mol. Catal. A* **2000**, *164*, 217.
(20) Wijzen, F.; Koch, B.; Rocha, J.; Esculcas, A.; Liegeois-Duyc-Kaerts, M.; Rulmont, A. *J. Catal.* **1998**, *177*, 96.
(21) Bautista, F. M.; Campelo, J. M.; Garcia, A.; Luna, D.; Marinas, J. M.; Romero, A. A.; Urbano, M. R. *J. Catal.* **1997**, *172*, 103.
(22) Bautista, F. M.; Campelo, J. M.; Garcia, A.; Luna, D.; Marinas, J. M.; Romero, A. A.; Siles, M. T. *Stud. Surf. Sci. Catal.* **2000**, *130*, 803.
(23) Bautista, F. M.; Bravo, M. C.; Campelo, J. M.; Garcia, A.; Luna, D.; Marinas, J. M.; Romero, A. A. *J. Mol. Catal. B* **1999**, *6*, 473.
(24) Bautista, F. M.; Campelo, J. M.; Garcia, A.; Jurado, A.; Luna, D.; Marinas, J. M.; Romero, A. A. *J. Mol. Catal. B* **2001**, *11*, 567.
(25) Brinker, C. J.; Cherer, G. W. *Sol−Gel Science*: *the Physics and Chemistry of Sol−Gel Processing*; Academic Press: San Diego, CA, 1990.
(26) Schneider, M.; Baiker, A. *Catal. Rev. Sci. Eng.* **1995**, *37*, 515.
(27) Miller, J. M.; Goodchild, M.; Lakshmi, L.; Wails, D.; Hartman, J. S. *Mater. Lett.* **2000**, *44*, 164.
(28) Maeda, K.; Mizukami, F.; Watanabe, M.; Arai, N.; Niwa, S. I.; Toba, M.; Shimizu, K. *J. Mater. Sci. Lett.* **1990**, *9*, 522.
(29) Maeda, K.; Mizukami, F.; Niwa, S. I.; Toba, M.; Watanabe, M.; Masuda, K. *J. Chem. Soc., Faraday. Trans.* **1992**, *88*, 97.
(30) Masuda, K.; Sano, T.; Mizukami, F.; Takezaki, T.; Kuno, K. *Appl. Catal. B* **1994**, *4*, 187.
(31) Zehl, G.; Bischoff, S.; Mizukami, F.; Isutzu, H.; Bartoszek, M.; Jancke, H.; Lucke, B.; Maeda, K. *J. Mater. Chem.* **1995**, *5*, 1893.
(32) Takenaka, S.; Takahashi, R.; Sato, S.; Sodesawa, T. *J. Sol-Gel Sci. Technol.* **2000**, *19*, 711.
(33) Froba, M.; Muth, O.; Reller, A. *Solid State Ionics* **1997**, *101*, 249.
(34) Pan, M.; Liu, J. R.; Lu, M. K.; Xu, D.; Yuan, D. R.; Chen, D. R.; Yang, P.; Yang, Z. E. *Thermochim. Acta* **2001**, *376*, 77.
(35) Miller, J. M.; Lakshmi, L. J. *J. Phys. Chem. B* **1998**, *102*, 6465.
(36) Miller, J. M.; Wails, D.; Hartman, J. S.; Belelie, J. S. *J. Chem. Soc., Faraday Trans.* **1998**, *94*, 789.
(37) Toba, M.; Mizukami, F.; Niwa, S. I.; Sano, T.; Maeda, K.; Shoki, H. *J. Mater. Chem.* **1994**, *4*, 1131.
(38) Mizukami, F.; Maeda, K.; Toba, M.; Sano, T.; Niwa, S. I.; Miyazaki, M.; Kojima, K. *J. Sol-Gel Sci. Technol.* **1997**, *8*, 101.
(39) Mizukami, F.; Kiyozumi, Y.; Sano, T.; Niwa, S. I.; Toba, M.; Shin, S. *J. Sol-Gel Sci. Technol.* **1998**, *10*, 1027.
(40) Yabuki, M.; Takahashi, R.; Sato, S.; Sodesawa, T.; Ogura, K. *Phys. Chem. Chem. Phys.* **2002**, *4*, 4830.
(41) Miller, J. M.; Rankin, S. E.; Ko, E. I. *J. Catal.* **1994**, *148*, 673.
(42) Zhuang, Q.; Miller, J. M. *Appl. Catal. A* **2001**, *209*, L1.
(43) Husing, N.; Launay, R.; Doshi, D.; Kickelbick, G. *Chem. Mater.* **2002**, *14*, 2429.
(44) Klimova, T.; Carmona, E.; Ramírez, J. *J. Mater. Sci.* **1998**, *33*, 1981.
(45) Toba, M.; Mizukami, F.; Niwa, S. I.; Kiyozumi, Y.; Maeda, K.; Annila, A.; Komppa, V. *J. Mater. Chem.* **1994**, *4*, 585.

materials prepared in the presence of a dihydroxylated organic compound have higher thermal stabilities and hence, larger surface areas, pore volumes, and surface acidities even after calcination at 1073−1273 K.

Experimental Section

Catalyst Preparation. $AlPO_4$ catalysts were obtained from $AlCl_3 \cdot 6H_2O$ and a phosphate source by precipitation with aqueous ammonia. Three phosphate sources were used: H_3PO_4 (85 wt %), $(NH_4)H_2PO_4$, and $(NH_4)_2HPO_4$, leading to $AlPO_4$ catalysts which were designated, respectively, as AP-H3, AP-H2, and AP-H1. The experimental procedure for AP-H2 from $(NH_4)H_2PO_4$ was as follows. A solution of 30.1 g of $(NH_4)H_2PO_4$ in 100 mL of deionized water was added drop by drop to a cold (273 K) solution containing 54.9 g of $AlCl_3 \cdot 6H_2O$ and 150 mL of deionized water, with continuous and vigorous stirring. Afterward, without interrupting the stirring process at 273 K, a cold diluted aqueous ammonia solution (40% volume) was added through use of an infusion pump (3 mL min^{-1}, Perfusor V, Braun) until the pH of the supernatant was 7. The white gel thus obtained was allowed to stand at room temperature for at least 18 h; the final pH after this time was 6.1. After filtration and several washings, first with deionized water and then with 2-propanol, the gel was dried at 393 K for 24 h and calcined at 773, 923, 1073, or 1273 K for 3 h. AP-H3 and AP-H1 catalysts were similarly synthesized by replacing $(NH_4)H_2PO_4$ with H_3PO_4 (85 wt %) and $(NH_4)_2HPO_4$, respectively. The catalysts thus obtained were designated as AP-H3, AP-H2, or AP-H1 followed by the calcination temperature (AP-H2-773, AP-H3-1073, and so on).

When an organic agent was present in the preparation step, it was stirred into the cool $AlCl_3 \cdot 6H_2O$ aqueous solution. The molar ratio organic agent/Al^{3+} was always 1. Four dihydroxylated organic agents were used: 1,2-ethanediol (ETD), 1,2-(12PRD) and 1,3-propanediol (13PRD), and 2-methyl-2,4-pentanediol (24PED). In all cases, the same washing and thermal treatments were used as in the case of AP-H2. Samples were denoted as AP followed by two hyphenated terms indicating, respectively, the organic agent and the calcination temperature (AP-ETD-923, AP-24PED-1073, and so on).

Characterization Methods. TGA and DTA were performed simultaneously using a Setaram Setsys 12 thermal station under an Ar flow (40 mL min^{-1}) and a heating rate of 10 K min^{-1}, from room temperature to 1473 K. Finely powdered α-alumina was used as a reference material. The samples used were the dried $AlPO_4$ material (393 K, 24 h) prior to calcination. Powder XRD diffraction patterns (5−75°, 2° min^{-1}) were recorded on a Siemens D-500 diffractometer (40 kV, 30 mA) using Ni-filtered Cu Kα radiation. Laser-Raman spectra were taken from slightly compacted samples at 3600−200 cm^{-1} (resolution 0.2 cm^{-1}), using a Perkin-Elmer System 2000 FT-Raman spectrometer. The laser power at the samples was in the range 5−100 mW. SEM-EPMA studies were carried out in a JEOL JSM-5400 apparatus coupled to a Link Isis Pentafet Model analyzer. Selected micrographs of many of the visual fields studied were reported here. XPS were recorded on a Leybold-Heraeus LHS-10 spectrometer (at 10^{-9} Torr) using Al Kα radiation and a pass energy constant of 50 eV. Binding energy values (accuracy, ±0.2 eV) were referred to as C(1s) peak (pollution carbon) at 284.6 eV. ^{27}Al (pulse 0.6 μs; recycle delay 0.3 s), ^{31}P (pulse 2.6 μs; recycle delay 6 s), and ^{1}H (pulse 3 μs; recycle delay 3 s) MAS NMR spectra were recorded at resonance frequencies ν_0 of 104.26, 161.98, and 400.13, respectively, with a Bruker ACP multinuclear spectrometer (external magnetic field of 9.4 T). No mathematical procedures were used, nor were the ^{27}Al chemical shifts corrected for second-order quadrupole effects. About 200 mg of sample material (previously dried at 413 K for at least 96 h) was used. The references for ^{27}Al, ^{31}P, and ^{1}H were $Al(H_2O)^{3+}$, 85 wt % H_3PO_4, and TMS, respectively. DRIFT spectra were recorded on a Bomem MB-100 FT-IR instrument equipped with an environmental chamber (Spectra Tech P/N 0030-101) placed in a diffuse reflectance attachment (Spectra Tech, Collector). A resolution of 8 cm^{-1} was used with 256 scans averaged to obtain a spectrum from 4000 to 400 cm^{-1}. Single beam spectra were ratioed against KBr collected at the same temperature as the sample. A plot of pseudo-absorbance was preferred. DRIFT spectra were recorded for all the calcined materials (200 mesh size and diluted to 15 wt % KBr) previously dried at 400 K for 24 h under vacuum. Afterward, the material was placed in the environmental chamber cell with a 20 mL min^{-1} flow of dehydrated and deoxygenated nitrogen, heated at 573 K and held at this temperature for 1 h prior to spectrum recording. In some cases, spectra were smoothed with a five-point Savitsky−Golay algorithm. N_2 adsorption measurements at 77 K were carried out on a Micromeritics ASAP 2000 analyzer after the samples were outgassed for 18 h at 393 K and 0.1 Pa. Surface areas were calculated according to the BET equation,[46] and total pore volume, V_P, was obtained from the amount adsorbed at a p/p_0 of about 0.99.[46] Mesopore size distributions were obtained using the BJH method and assuming a cylindrical pore model. The analysis was applied to the adsorption branch of each isotherm which is preferred to the desorption branch for type IV isotherms.[47] The absence of micropores was determined by the *t*-plot method, using the Harkins−Jura correlation[48] for *t* as a function of p/p_0. Parameters were fitted to low-area, nonporous silica. Surface acidity was measured in a dynamic mode[49,50] by means of the gas-phase adsorption of pyridine (PY) and 2,6-dimethylpyridine (DMPY) at 473 and 573 K, using a pulse technique described elsewhere.[51] The pulse size was in the range of gas chromatography linearity, corresponding to 0.1−0.5 monolayer.

Catalytic Measurements. Cyclohexene conversion was carried out in a microcatalytic pulse reactor, inserted between the sample inlet and the analytical column of a HP-5890 GC, according to a method previously described.[51] The pulse size was within the linear range of the adsorption isotherm. Catalytic measurements were performed under the following conditions: cyclohexene (liquid) volume/pulse, 1 μL; catalyst weight, 20−50 mg; temperature, 523−673 K (50-K intervals); flow rate of N_2 (99.999%, H_2O < 3 ppm) carrier, 40 mL min^{-1}; GC (at 323 K) with FID and two columns (1/8 in., stainless steel) in series packed with, respectively, 5% polyphenyl ether (six rings) on Chromosorb G AW-DMCS 80/100 (2 m) and 5% squalane on Chromosorb P-AW 60/80 (3 m). The reaction products, characterized by GC-MS (HP-5970 MSD detector; 60 m SPB-1 capillary column at 308 K), were 1- and 3-methylcyclopentene (1- and 3-MCP). Cyclohexene (Aldrich, p.a.) was used after two distillation processes and further purification with a column of alumina previously calcined at 573 K for 3 h.

Results and Discussion

TG/DTA Measurements. TG and DTA profiles for the AP-H2 sample are shown in Figure 1. AP-H1 and AP-H3 samples displayed practically the same behavior. TG profiles were characterized by two weight losses up to 650 K. The first one (ca. 15%), at 293−500 K, accompanied by a DTG peak (∼415 K) and an endothermic DTA band (∼408 K), was due to desorption of physically adsorbed water and 2-propanol. The second

(46) Sing, K.; Everett, D. H.; Haul, R. A. W.; Moscou, L.; Pierotti, R. A.; Rouquerol, J.; Siemieniewska, T. *Pure Appl. Chem*. **1985**, *57*, 603.

(47) Broekhoff, J. C. P.; Linsen, B. G. In *Physical and Chemical Aspects of Adsorbents and Catalysts*; Linsen, B. G., Ed.; Academic Press: London, 1970; p 1.

(48) Harkins, W. D.; Jura, G. *J. Chem. Phys*. **1943**, *11*, 431.

(49) Ghosh, A. K.; Curthoys, G. *J. Chem. Soc., Faraday Trans. 1* **1983**, *29*, 2569

(50) Paryjczak, T. *Gas-Chromatography in Adsorption and Catalysis*; Wiley: New York, 1986.

(51) Campelo, J. M.; Garcia, A.; Luna, D.; Marinas, J. M. *J. Mater. Sci*. **1990**, *25*, 2513.

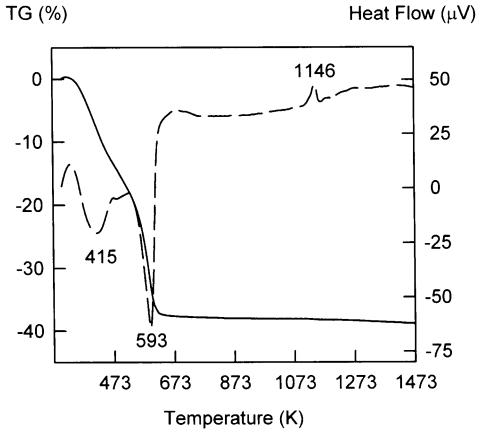

Figure 1. TG and DTA profiles for AP-H1 sample. Static air atmosphere; scan: 10 K min^{-1}.

weight loss (ca. 22%), at 500−650 K, also accompanied by a DTG peak (∼593 K) and an endothermic DTA band (∼588 K) was due to the removal of occluded ammonium chloride. Between 650 and 1473 K, a slight weight loss was observed, due mainly to the condensation of surface hydroxyls, together with an exothermic DTA peak (without a corresponding DTG peak). The position of this band remained almost unchanged with the phosphate source: AP-H3 (1140 K), AP-H2 (1146 K), and AP-H1 (1152 K). Because of the temperature dependence of the $AlPO_4$ XRD patterns (see below), the exothermic peak was deduced to come from phase transformation of amorphous $AlPO_4$ to a crystalline α-cristobalite $AlPO_4$.

TG profiles (not shown) of $AlPO_4$ materials obtained in the presence of an organic agent exhibited a third weight loss in the 298−650 K range, accompanied by a DTG peak (∼490 K) and an endothermic DTA band (∼483 K) that was attributed to the decomposition and removal of occluded organics. In addition, there was also a slight weight loss in the 650−1473 K range due to the hydroxyl condensation that was also accompanied by an exothermic DTA peak. However, the position of these bands shifted toward higher temperatures in relation to the respective $AlPO_4$ material (AP-H3) obtained in the absence of the organic diol. The temperatures of the exothermic peaks were as follows: AP-ETD, 1238 K; AP-12PRD, 1246 K; AP-13PRD, 1350 K; and AP-24PED, 1403 K. So, the crystallization of the $AlPO_4$ was delayed, showing higher thermal stability when dihydroxylated organic compounds were used as aluminum chelating agents in the preparatory step.

XRD Measurements. *APH3, AP-H2, and AP-H1 Materials.* Figure 2 shows the XRD patterns of AP-H2 material calcined at different temperatures (773−1273 K). AP-H3 and AP-H1 exhibited the same behavior. Materials calcined at 773 and 923 K exhibited only a very broad band in the 2θ range from 15° to 30° (Figure 2, curves a−b), a characteristic of the amorphous $AlPO_4$. Thermal treatment at 1073 K developed bands corresponding to crystalline $AlPO_4$ (Figure 2, curve c) that turned into fully crystallized $AlPO_4$ (Figure 2, curve d) when heated at 1273 K. Thus, in those materials thermally treated at 1273 K or after DTA measurements (1473 K), bands were observed (identified from the ASTM index 11-0500) corresponding to the orthorhombic symmetry of α-cristobalite $AlPO_4$ [$2\theta = 21.8$ ($d =$ 4.075 Å), $2\theta = 28.2$ ($d = 3.159$ Å), $2\theta = 30.8$ ($d = 2.869$ Å), and $2\theta = 35.8$ ($d = 2.503$ Å)]. The small peak at $2\theta = 20.6$ ($d = 4.313$ Å) was incompatible with the orthorhombic symmetry of α-cristobalite, but may be related to the presence of structural defects according to Florke.[52] Moreover, XRD profiles after DTA analysis did not show any product of aluminum segregation. So, we can establish that the exothermic transition around 1145 K did therefore correspond to crystallization from the amorphous mass to crystallized $AlPO_4$.

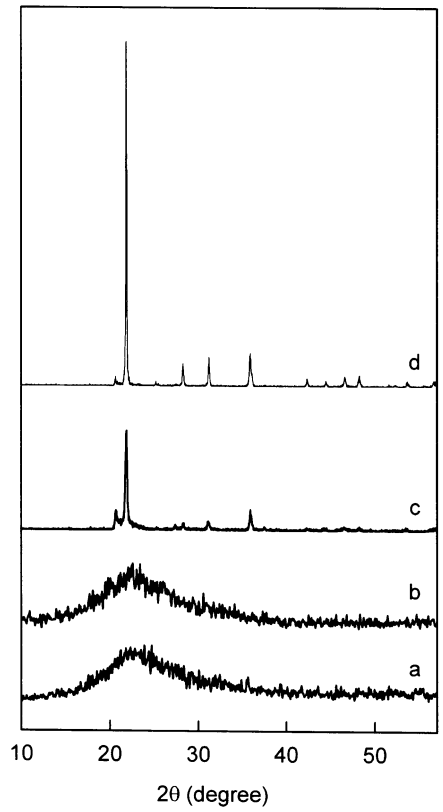

Figure 2. X-ray diffraction patterns (Cu Kα, $\lambda = 1.5405$ Å) of AP-H2-773 (a), AP-H2-923 (b), AP-H2-1073 (c), and AP-H2-1273 (d) materials.

$AlPO_4$ Materials Obtained in the Presence of an Al-Complexing Agent. XRD analysis of all $AlPO_4$ materials calcined at temperatures below 1273 K indicated that amorphous materials were formed for every organic agent. Thermal treatment at 1273 K developed fully crystallized $AlPO_4$ in AP-ETD and AP-12PRD materials, exhibiting bands corresponding to the orthorhombic symmetry of α-cristobalite $AlPO_4$ (Figure 3, curves a−b), while a small degree of crystallization was found in AP-13PRD material (Figure 3, curve c). The bands corresponded to a mixture of tridymite and α-cristobalite although with a small degree of crystallinity. Pseudohexagonal tridymite was identified by its characteristic reflections at $2\theta = 20.4$ ($d = 4.348$ Å), $2\theta = 21.6$ ($d =$ 4.110 Å), and $2\theta = 23.2$ ($d = 3.830$ Å) [ASTM 20-45]. The mixture of tridymite and α-cristobalite is enriched in the α-cristobalite phase as thermal treatment temperature increases. Thus, after DTA measurements (1473 K), only the α-cristobalite phase is found. The AP-24PED material remained amorphous even at 1273 K (Figure 3, curve d). After DTA analysis (1473 K),

(52) Florke, O. W. *Z. Kristallogr.* **1967**, *125*, 1934.

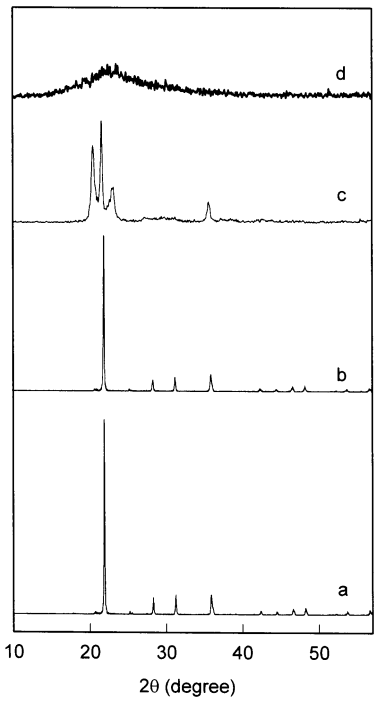

Figure 3. X-ray diffraction patterns (Cu Kα, $\lambda = 1.5405$ Å) of AP-ETD-1273 (a), AP-12PRD-1273 (b), AP-13PRD-1273 (c), and AP-24PED-1273 (d) materials.

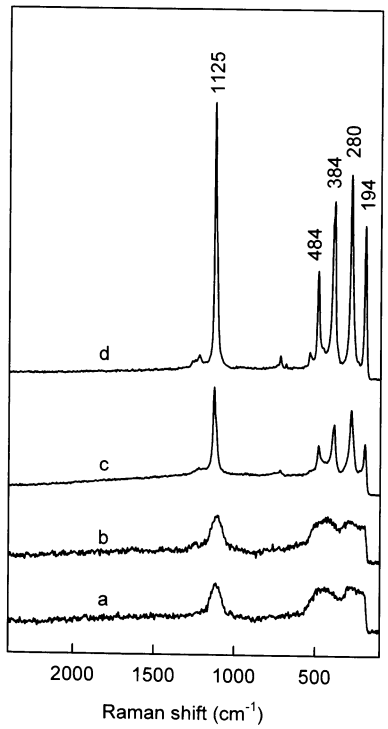

Figure 4. Laser-Raman spectra of AP-H1-773 (a), AP-H1-923 (b), AP-H1-1073 (c), and AP-H1-1273 (d) materials.

however, they also crystallize like AP-13PRD material. Furthermore, the XRD analysis carried out immediately before the DTA exotherm showed that all $AlPO_4$ materials remained amorphous. So, exothermic transitions really corresponded to a crystallization process.

Laser-Raman Spectra. Figure 4 shows the Raman spectra of AP-H1 materials (AP-H3 and AP-H2 exhibited the same behavior). Curves a and b, related to samples calcined below 1073 K, confirm the bulk datum

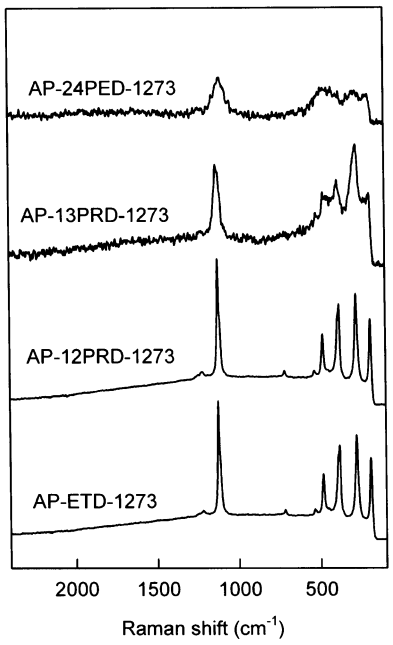

Figure 5. Laser-Raman spectra of AP-ETD-1273 (a), AP-12PRD-1273 (b), AP-13PRD-1273 (c), and AP-24PED-1273 (d) materials.

given by XRD with respect to the still amorphous nature of $AlPO_4$ material. Curves c and d confirm XRD results that $AlPO_4$ is crystalline and belongs to the α-cristobalite form. The spectra of AP-H1-1273 reveal five bands at 1125, 484, 384, 280, and 194 cm^{-1}. In this respect, Handke et al.[53,54] measured the Raman spectra of polymorphic forms of $AlPO_4$ (berlinite, cristobalite, and tridymite) by using the tetrahedral anion model of $[PO4]^{3-}$ tetrahedron isolated by Al^{3+} ions. Above 200 cm^{-1}, they found four bands for the orthorhombic α-cristobalite phase, at 1124, 488, 390, and 284 cm^{-1}. Thus, bands observed in Figure 4 (curve d) were unambiguously assigned to the α-cristobalite $AlPO_4$ phase.

Raman spectra (Figure 5) of $AlPO_4$ materials obtained in the presence of organic agents also corroborated the XRD measurements. Thus, only those materials thermally treated at 1273 K exhibited Raman bands, with the exception of AP-24PED-1273. These bands were fully developed for AP-ET-1273 and AP-12PRD-1273 materials (Figure 5, curves a−b) whereas those for AP-13PRD-1273 were poorly resolved (Figure 5, curve c), although the band at 1133 cm^{-1} indicated the presence of an $AlPO_4$ tridymite phase, thus confirming XRD results. After DTA analysis (1473 K), only the α-cristobalite phase was found. The AP-24PED material remained very poorly resolved even at 1273 K (Figure 5, curve d) although the α-cristobalite $AlPO_4$ phase was also found after DTA analysis.

^{27}Al and ^{31}P MAS NMR Measurements. The ^{27}Al MAS spectra of all amorphous $AlPO_4$ materials (Figure 6; AP-H2 as an example) showed the presence of a sole broad peak around 36 ppm, typical of tetrahedral Al with P in the second coordination sphere, i.e., sharing

(53) Handke, M.; Mozgawa, W.; Rokita, M. *Mikrochim. Acta Suppl.* **1997**, *14*, 511.
(54) Rokita, M.; Handke, M.; Mozgawa, W. *J. Mol. Struct.* **2000**, *555*, 351.

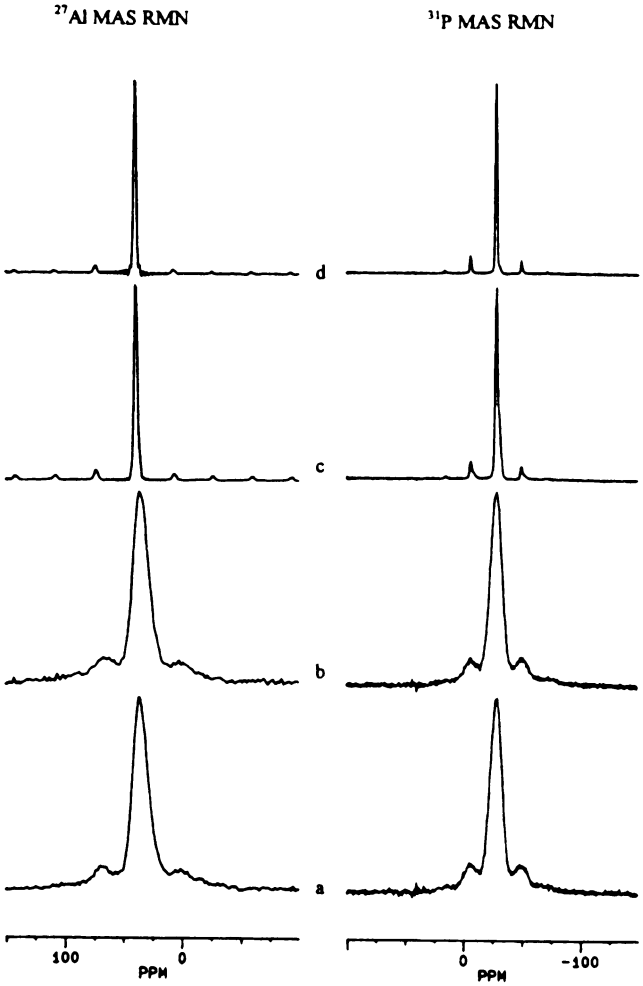

Figure 6. ^{27}Al (104.26 MHz) and ^{31}P (161.98 MHz) MAS NMR spectra of AP-H2-773 (a), AP-H2-923 (b), AP-H2-1073 (c), and AP-H2-1273 (d) materials.

oxygens with four phosphorus tetrahedra [$Al(OP)_4$].[55−58] The strong upfield shift observed with respect to other aluminum oxides is attributed by Muller et al.[55] to the influence of P atoms located in the second coordination sphere of Al. Moreover, the ^{31}P MAS spectra (Figure 6) also exhibited a sole single component at around −29 ppm that corresponded to P atoms in tetrahedral coordination with P−O−Al bonds, i.e., $P(OAl)_4$ environments. Furthermore, it appears that the chemical shifts of P at different sites are similar, resulting in a broadened peak. As the crystallinity of the $AlPO_4$ material increased, both ^{27}Al and ^{31}P signals narrowed and shifted to a lower field, to 40.2 and −27.5 ppm, respectively, for $AlPO_4$ in crystalline α-cristobalite polymorph (Figure 6d). In the case of AP-24PED-1273, neither ^{27}Al nor ^{31}P signals narrowed, thus strengthening its amorphous nature. In this respect, Kanehashi and Saito,[59] used $^{17}O \rightarrow {}^{31}P$ CP/MAS NMR to show that ^{31}P chemical shifts were sensitive to the condensation degree of PO_4 units. Therefore, there were at least three

Table 1. Electron Microprobe Analysis and XPS Binding Energies[a] of the Elements Present on the Surface of $AlPO_4$ Materials

material	P(2p) (at. %)	Al(2p) (at. %)	O(1s) (at. %)	P/Al
APH3-923	15.80 (133.5)	17.88 (74.1)	66.32 (531.5)	0.88
AP-H3-1273	15.72 (133.8)	18.00 (74.1)	66.28 (531.6)	0.87
AP-H2-923	17.71 (134.3)	18.00 (74.1)	66.29 (532.0)	0.87
AP-H2-1273	15.62 (134.1)	18.15 (74.1)	66.23 (531.9)	0.86
APH1-923	15.81 (134.1)	18.00 (74.1)	66.20 (531.9)	0.88
AP-H1-1273	15.80 (133.9)	17.90 (74.1)	66.29 (532.0)	0.88
AP-ETD-923	15.62 (134.1)	18.13 (74.1)	66.25 (531.9)	0.86
AP-12PRD-923	15.51 (133.9)	18.28 (74.1)	66.20 (531.6)	0.85
AP-13PRD-923	15.69 (133.8)	18.04 (74.1)	66.28 (531.6)	0.87
AP-13PRD-1273	15.64 (134.0)	18.10 (74.1)	66.26 (531.7)	0.86
AP-24PED-923	15.84 (134.4)	17.83 (74.1)	66.34 (532.1)	0.89
AP-24PED-1273	15.82 (134.1)	17.90 (74.1)	66.28 (532.0)	0.88

[a] In parentheses, eV.

different phosphorus environments in amorphous $AlPO_4$, prepared by neutralizing an aqueous solution of $Al(NO_3)_3 \cdot 9H_2O$ and ^{17}O-enriched H_3PO_4 at a controlled pH of 8 using ammonium hydroxide. The phosphorus environments depended on the condensation degree of PO_4 tetrahedral units, denoted Q^n (n is the number of oxygen atoms shared with the next PO_4 unit). Thus, authors assigned the peaks to −14, −23, and −30 ppm [$(NH_4)_2HPO_4$ as ^{31}P reference] to Q^2, Q^3, and Q^4 units. Moreover, during the thermal treatment of all $AlPO_4$ up to 1273 or 1473 K, aluminum was not segregated as Al_2O_3.[57] Similar results concerning Al and P arrangements in amorphous compounds, obtained during coprecipitation of aluminophosphate catalysts with different P/Al ratios, have been reported by Cheung et al.[58]

Furthermore, the ^1H MAS spectra (not shown) of amorphous $AlPO_4$ contained a small line from Al−OH groups (ca. $\delta = 0.9$ ppm) and an unresolved peak from P−OH groups (ca. $\delta \sim 3.6$ ppm) as described by Mastikhin et al.[60] In addition, the peak at $\delta \sim 3.6$ ppm decreased in intensity with calcination temperature. For crystalline $AlPO_4$ materials, both ^1H signals disappeared. These results were confirmed by DRIFT spectroscopy (see below).

SEM, EPMA, and XPS Studies. SEM micrographs of different $AlPO_4$ materials that calcined at 923 K are shown in Figure 7 (a, c−f). SEM observation showed a very widely varied distribution in morphology, texture, and particle sizes for all $AlPO_4$ materials. No great changes were observed either in morphology or in particle size when organic agents were used. The average size of the biggest particles was around 50 μm, although a large population of small particles was observed in all samples. The situation remained almost unchanged for all amorphous $AlPO_4$ materials, regardless of the calcination temperature and organic agent used. However, a modification in surface texture together with a great increase in particle size was found in crystalline $AlPO_4$ materials (small particles disappeared), as can be observed in Figure 7b.

Table 1 summarizes the information about the elemental surface composition (EPMA) and XPS binding energies (in parentheses) of the elements present on the surface of $AlPO_4$ materials. Microanalysis (EPMA) of the surface showed a very homogeneous distribution of P

(55) Muller, D.; Janh, E.; Ladwig, G.; Haubenreisser, U. *Chem. Phys. Lett.* **1984**, *109*, 332.
(56) Blackwell, C. S.; Paton, R. L. *J. Phys. Chem.* **1984**, *88*, 6135.
(57) Sanz, J.; Campelo, J. M.; Marinas, J. M. *J. Catal.* **1991**, *130*, 642.
(58) Cheung, T. T. P.; Willcox, K. W.; McDaniel, M. P.; Johnson, M. M.; Bronnimann, C.; Frye, J. *J. Catal.* **1986**, *102*, 10.
(59) Kanehashi, K.; Saito, K. *Chem. Lett.* **2002**, 668.
(60) Mastikhin, V. M.; Mudrakowsky, I. L.; Shmachkova, V. P.; Kotsarenko, N. S. *Chem Phys. Lett.* **1987**, *139*, 93.

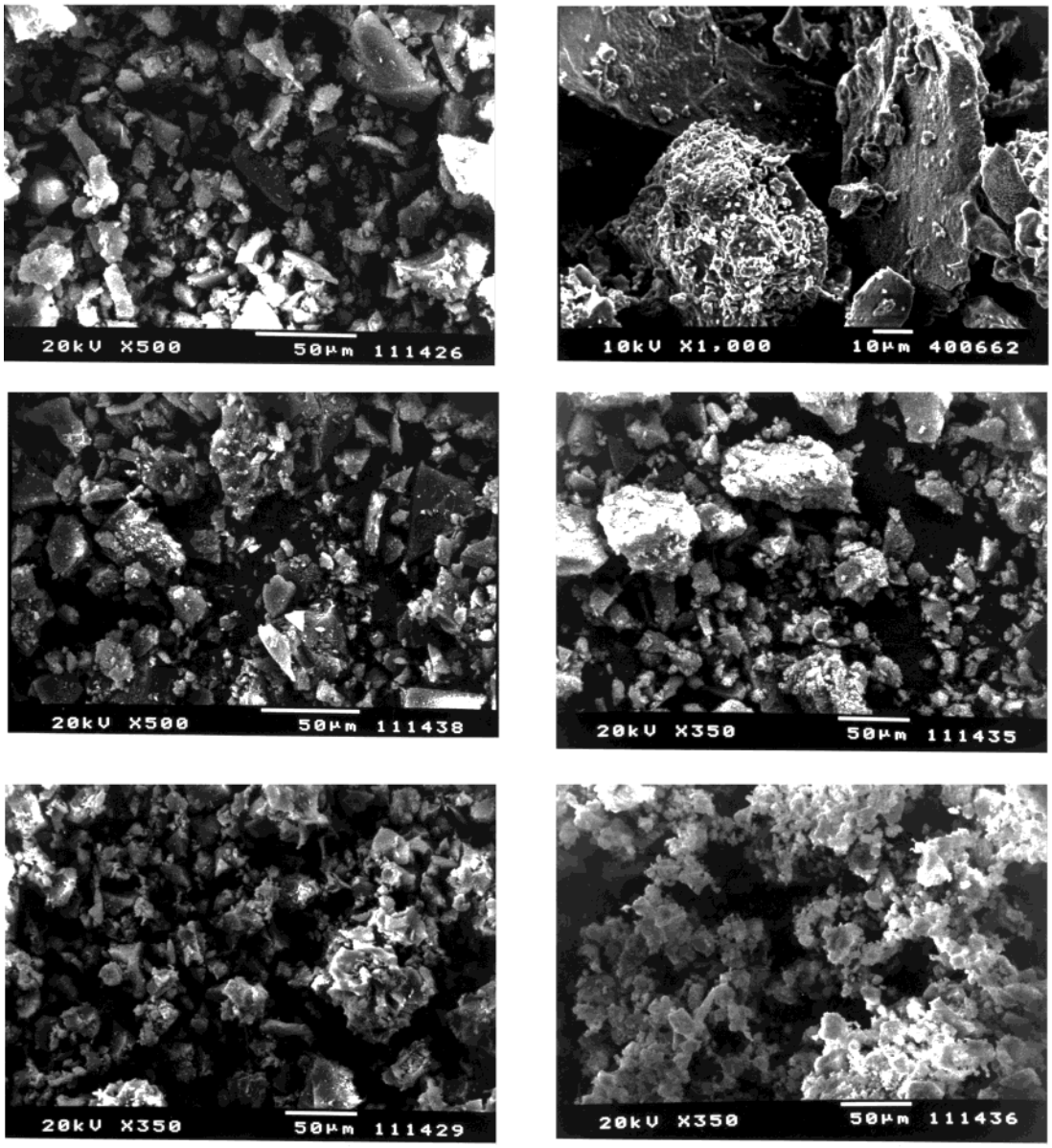

Figure 7. SEM micrographs of AP-H1-923 (a), AP-H1-1273 (b), AP-ETD-923 (c), AP-12PRD-923 (d), AP-13PRD-923 (e), and AP-24PED-923 (f) materials.

and Al, not only within the particles, but also between them. As can be seen in Table 1, the surface concentration ratio P/Al of $AlPO_4$ materials remained almost constant, regardless of their amorphous or crystalline nature, and it also showed surface enrichment in Al when compared to bulk values. This also occurred when $AlPO_4$ materials were obtained with ethylene or 1,2-propylene oxides instead of aqueous ammonia.[17] Furthermore, the core lines investigated for different samples were very similar and appeared as single symmetrical lines, indicating a homogeneous distribution in the electron densities around the atoms throughout the solid.

DRIFT Measurements. Figures 8 and 9 show the DRIFT spectra of thermally treated AP-H2 and AP-13PRD materials, recorded after pretreatment at 573 K (1 h) under a nitrogen stream (30 mL min^{-1}). Two isolated hydroxyl peaks were found in the OH stretching region: a weak one at 3786 cm^{-1} and a strong one at 3674 cm^{-1}. These were due to surface Al−OH groups (with Al atoms in tetrahedral coordination) and nonbonded surface P−OH ones, respectively.[61−63] There was also a broad band around 3540 cm^{-1} due to surface hydroxyl groups, most likely phosphorus ones, perturbed by a hydrogen bridge bond from a surface hydroxyl band. As can be seen in Figures 8 and 9, an increase in the calcination temperature resulted in the gradual disappearance of Al−OH and P−OH bands. Thus, in those $AlPO_4$ materials obtained in the absence of an organic agent (Figure 8), the Al−OH and P−OH surface groups were removed at calcination temperatures of 1073 K, regardless of the phosphate source.

Regarding the $AlPO_4$ obtained in the presence of an organic agent, the Al−OH and P−OH surface groups still remained at 1073 K (Figure 9, curves a−c), al-

(61) Peri, J. B. *Discuss. Faraday Soc.* **1971**, *52*, 55.
(62) Farmer, V. C. *The Infrared Spectra of Minerals*; Butterworths: London, 1974.
(63) Arlidge, E. Z.; Farmer, V. C.; Mitchell, B. C.; Mitchell, W. A. *J. Appl. Chem.* **1963**, *13*, 17.

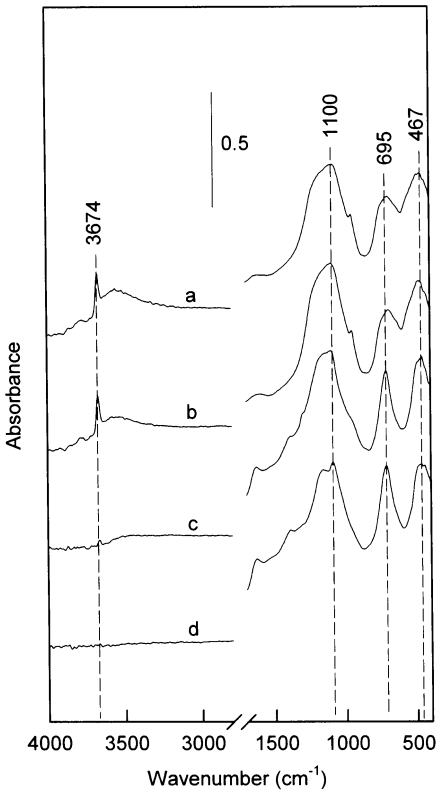

Figure 8. DRIFT spectra recorded at 573 K in a nitrogen stream (20 mL min^{-1}) for AP-H2-773 (a), AP-H2-923 (b), AP-H2-1073 (c), and AP-H2-1273 (d) materials.

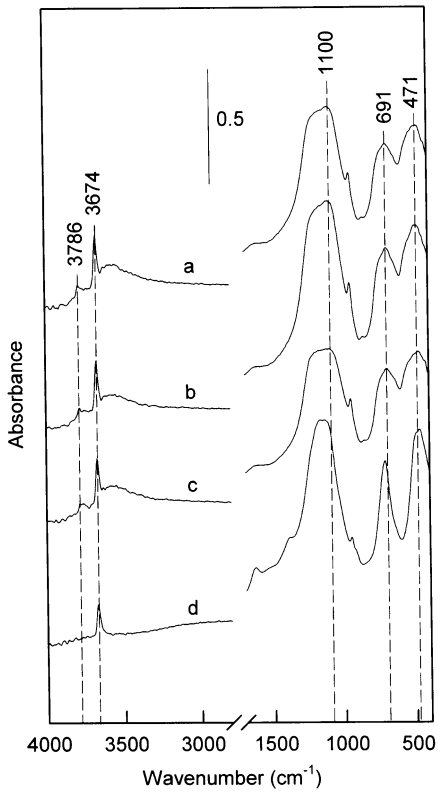

Figure 9. DRIFT spectra recorded at 573 K in a nitrogen stream (20 mL min^{-1}) for AP-13PRD-773 (a), AP-13PRD-923 (b), AP-13PRD-1073 (c), and AP-13PRD-1273 (d) materials.

though on treatment at 1273 K, both surface hydroxyl groups disappeared completely for AP-ETD-1273 and AP-12PRD-1273 materials (due to crystallization into α-cristobalite $AlPO_4$ phase). On the other hand, the isolated P−OH groups were still present for AP-13PRD-1273 material, due to their poor crystalline structure (Figure 9, curve d). Moreover, in AP-24PED-1273 material the population of isolated Al−OH and P−OH groups decreased slightly when compared to that of AP-24PED-773, reaffirming the amorphous nature of such materials. Furthermore, the DRIFT spectra in the skeletal region (below 1700 cm^{-1}) showed that the P atom in all $AlPO_4$ materials was surrounded by tetrahedra of oxygen atoms: bands due to triply degenerate P−O stretching vibration (∼1100 cm^{-1}) ν_3 mode of tetrahedral PO_4^{3-}; triply degenerate O−P−O bending vibration (∼470 cm^{-1}) ν_4 mode of PO_4^{3-} tetrahedra, and stretching vibration of Al−O bonds in combination with P−O bonds (∼690 cm^{-1}). So, DRIFT data agreed with the XRD, laser-Raman, and ^{27}Al and ^{31}P MAS NMR data.

Table 2. Textural Properties of $AlPO_4$ Materials

material	S_{BET} ($m^2\ g^{-1}$)	V_p (mL g^{-1})	d_P (nm)	ΣV_p (mL g^{-1})	ΣS_P ($m^2\ g^{-1}$)
AP-H1-773	180	0.99	21.7	0.99	189
AP-H1-923	187	0.98	20.9	0.99	198
AP-H1-1073	6				
AP-H1-1273	1				
AP-H2-773	190	0.85	17.0	0.84	188
AP-H2-923	193	0.87	17.9	0.87	207
AP-H2-1073	3				
AP-H2-1273	1				
AP-H3-773	197	0.83	15.9	0.83	192
AP-H3-923	196	0.83	16.8	0.83	212
AP-H3-1073	2				
AP-H3-1273	1				
AP-ETD-773	209	1.18	22.4	1.18	209
AP-ETD-923	219	1.15	20.9	1.15	225
AP-ETD-1073	212	1.13	21.1	1.14	222
AP-ETD-1273	1				
AP-12PRD-773	195	1.20	23.8	1.20	205
AP-12PRD-923	212	1.15	21.1	1.16	221
AP-12PRD-1073	197	1.09	21.8	1.10	209
AP-12PRD-1273	1				
AP-13PRD-773	227	1.34	20.0	1.26	222
AP-13PRD-923	231	1.45	24.2	1.45	241
AP-13PRD-1073	249	1.50	21.8	1.48	252
AP-13PRD-1273	44	0.79	41.6	0.64	42
AP-24PED-773	221	1.54	25.2	1.50	252
AP-24PED-923	219	1.65	28.5	1.64	285
AP-24PED-1073	205	1.45	26.6	1.43	266
AP-24PED-1273	203	1.39	25.9	1.37	211

Textural Properties. *APH3, AP-H2, and AP-H1 Materials.* In all of these materials, treatment temperatures up to 923 K resulted in N_2 isotherms (not shown) with closed and well-defined hysteresis loops. The isotherms were Type IV exhibiting H1 hysteresis loops which corresponded to solids with mesoporous textures.[46] In addition, *t*-plots (not shown) from the isotherm adsorption branch showed the absence of microporosity. Also, the surface areas calculated by the *t*-method, from the slope of the straight lines extrapolated through the origin, were found to tally with those obtained using the BET method. This reflected not only how free of micropores the samples were, but also the great degree of accuracy in C_{BET} determination. After heating at 1073 K, these materials displayed reversible Type II isotherms that corresponded to nonporous adsorbents. The main pore texture characteristics (S_{BET}, pore volumes, and average pore diameters) are reported in Table 2. The cumulative surface area (ΣS_P) and pore volume (ΣV_P) were comparable to the corresponding measured values of S_{BET} and V_P. This agreement

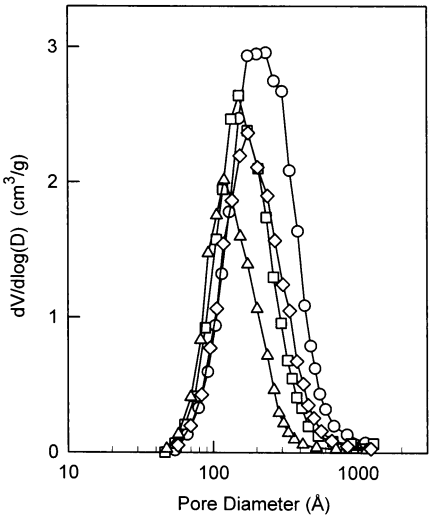

Figure 10. BJH pore size distributions for AP-H1-923 (△), AP-ETD-923 (□), AP-12PRD-923 (◇), and AP-24PED-923 (○) materials.

indicated that the method chosen for pore analysis was appropriate.

Textural properties confirmed the sintering process in solids over 923 K, which accompanied $AlPO_4$ crystallization (see above). Thus, S_{BET} and mesopore volume remained almost unchanged as calcination temperature increased from 773 to 923 K, although they dropped dramatically when calcination temperature increased. Moreover, the phosphorus source had practically no effect on the textural properties in $AlPO_4$ materials. However, materials obtained from H_3PO_4 exhibited slightly higher pore volumes and pore diameters than those materials obtained from $(NH_4)H_2PO_4$ and $(NH_4)_2HPO_4$, although they did exhibit somewhat smaller surface areas. The pore size distribution was found to be monomodal for all mesoporous materials, showing a relatively broad spectrum of pore size with well-defined maxima in the mesopore region.

$AlPO_4$ Materials Obtained in the Presence of an Al-Complexing Agent. There is a detailed analysis of the N_2 isotherms in these materials in Table 2. The most striking feature of the results shown in Table 2 was that the presence of a complexing agent strongly influenced the development of textural properties with respect to temperature when compared to $AlPO_4$ material obtained in the absence of an organic agent (AP-H3). So, all materials calcined at 1073 K maintained a mesoporous texture (type IV isotherms with H1 hysteresis loops). On the other hand, as can be seen in Table 2, S_{BET} and V_P remained almost unchanged as calcination temperature increased from 773 to 1073 K. A decrease in these values was observed, however, when calcination temperature increased to 1273 K. This effect depended on the organic agent added. Thus, a significant decrease in surface area (from 190−200 to 1 $m^2\ g^{-1}$) was found for AP-ETD and AP-12PRD materials (revealing shrinkage of the pore structure), whereas the decrease was less for AP-13PRD. However, textural properties in AP-24PED materials remained practically unaltered at calcination temperatures in the range 773−1273 K. N_2 adsorption studies indicated much higher pore volumes in the case of AP-13PRD and AP-24PED materials. Furthermore, pore size distributions (Figure 10) were displaced toward larger pores and were quite broad, as indicated by the great width halfway up the peaks.

So, the results indicated that $AlPO_4$ materials prepared in the presence of an Al-complexing agent had better textural properties (larger surface areas, pore volumes, and pore diameters) than the $AlPO_4$ obtained without such an agent under identical conditions. These facts were important because this modification in the surface texture of $AlPO_4$, caused by the organic agent, was accompanied by steady surface acidity, and hence, catalytic activity for cyclohexene skeletal isomerization (see below).

These results could be explained assuming that the presence of a diol as the organic ligand strongly changed the formation process of the primary aluminum phosphate gel. The varying conditions during the gel's formation resulted in different organic−inorganic interactions, degrees of distortion, and degrees of polymerization in the structural units (for instance, a shortening of polyphosphate chains terminated with P−OH groups). These lessened the tendency to form bulky gels, and favorably enhanced the formation of a specific hydrous $AlPO_4$ gel structure. This structure was less cross-linked and exhibited bigger pores due to a better adjustment of the phosphate anion and chelated aluminum condensation rates, different concentrations of OH groups, and hence, different behavior with respect to thermal treatment (drying and calcination) and crystallization. The formation of this specific polymeric network allowed the gel to undergo a series of chemical and physical changes on subsequent drying and calcination that led to a more thermally stable $AlPO_4$ structure with better textural properties. As a result, $AlPO_4$ materials still retained a mesoporous structure with a relatively large surface area and porosity even at 1073/1273 K calcination temperatures, unlike the $AlPO_4$ obtained in the absence of an organic agent.

Moreover, the molecular structures of the four organic agents had the same hydrophilic OH groups, although they did differ in the number and steric hindrance of their hydrophobic groups. The hydrophilic and hydrophobic groups together with steric hindrance should play an important, although complex, role in directing the cross-linked polymeric mesoporous network and in determining the final textural parameters of the $AlPO_4$ materials synthesized with an organic agent. The data indicated that 1,3-diols (13PRD and 24PED) were better agents than 1,2-diols (12ETD and 12PRD), thus leading to $AlPO_4$ materials exhibiting excellent thermal stability and mesoporosity. In fact, all the pore parameters for the former materials were superior to those for the latter ones. In this sense, bulky diols, like 24PED, represented very suitable modifying ligands for the preparation of amorphous SiO_2,[31] Al_2O_3,[28−30] and SiO_2−Al_2O_3[39] materials with high surface areas and larger pore volumes and pore diameters, even after calcination at high temperature. However, strong complexing agents, such as nonbranched diols, yielded an Al_2O_3 crystallizing to α-phase at low temperature.[29] The authors explain these results on the basis of stability of the aluminum chelates. Thus, 1,2-diols form five membered ring chelates while 1,3-diols form six-membered ring chelates. Generally, the former were more stable thermodynamically than the latter.[64] Besides, on comparing

Table 3. Surface Acidity of $AlPO_4$ Catalysts

	PY (μmol g^{-1})[a]		DMPY (μmol g^{-1})[a]	
catalyst	473 K	573 K	473 K	573 K
AP-H1-773	124 (0.68)	*b*	69 (0.38)	6 (0.03)
AP-H1-923	89 (0.48)	*b*	*b*	*b*
AP-H1-1073	*c*			
AP-H2-773	113 (0.59)	*b*	61 (0.32)	7 (0.03)
AP-H2-923	91 (0.47)	*b*	*b*	*b*
AP-H2-1073	*c*			
AP-H3-773	104 (0.53)	7 (0.04)	67 (0.34)	6 (0.03)
AP-H3-923	82 (0.42)	*b*	*b*	*b*
AP-H3-1073	*c*			
AP-ETD-773	111 (0.53)	8 (0.04)	71 (0.34)	7 (0.03)
AP-ETD-923	85 (0.39)	*b*	39 (0.18)	2 (0.01)
AP-ETD-1073	79 (0.37)	*b*	*b*	*b*
AP-ETD-1273	*c*			
AP-12PRD-773	117 (0.60)	11 (0.06)	75 (0.38)	7 (0.04)
AP-12PRD-923	112 (0.53)	10 (0.05)	63 (0.30)	3 (0.01)
AP-12PRD-1073	106 (0.54)	10 (0.05)	*b*	*b*
AP-12PRD-1273	*c*			
AP-13PRD-773	137 (0.60)	15 (0.07)	78 (0.34)	9 (0.04)
AP-13PRD-923	100 (0.43)	9 (0.04)	77 (0.33)	5 (0.02)
AP-13PRD-1073	80 (0.32)	8 (0.03)	*b*	*b*
AP-13PRD-1273	63 (1.40)	6 (0.13)	*b*	*b*
AP-24PED-773	135 (0.62)	23 (0.10)	85 (0.39)	11 (0.05)
AP-24PED-923	124 (0.57)	19 (0.09)	81 (0.37)	7 (0.03)
AP-24PED-1073	115 (0.56)	18 (0.09)	80 (0.39)	5 (0.02)
AP-24PED-1273	115 (0.57)	18 (0.09)	70 (0.35)	4 (0.02)

[a] Acid density in parentheses (μmol m^{-2}). [b] Not measured. [c] There is no adsorption of the probe molecule.

13PRD and 24PED, the 13PRD chelate was more stable than that of 24PED, because the two methyl groups on the carbon of the 2-position in 24PED caused great steric hindrance. Thus, the utilization of bulky 1,3-diols, like 24PED, as organic additives led to $AlPO_4$ catalysts with an improved thermal stability and hence, better textural properties.

Furthermore, with respect to $AlPO_4$ materials[3] prepared by a reversed microemulsion assisted procedure [with a similar P/Al ratio but using a different aluminum source, i.e. $Al(NO_3)_3 \cdot 9H_2O$, at a calcination temperature of 873 K], AP-24PED materials exhibited smaller specific surface areas (219 vs 370 m^2 g^{-1}). Their pore volumes (1.65 vs 0.95) and pore diameters (28 vs 7 nm), however, were substantially greater, exhibiting also a broader pore size distribution. The authors have not included details about the evolution of surface area and pore properties of solids calcined at temperatures over 873 K.

Surface Acidity Measurements. Gas-chromatographic pulse techniques could provide surface acidity information at catalytic reaction temperatures[49,50] but were unable to distinguish Bronsted and Lewis sites unless specific basic probes were used. Moreover, it is known that DMPY is selectively in Bronsted-acid sites, but not in Lewis-acid sites because of a steric hindrance of two methyl groups,[65−67] whereas sterically nonhindered PY is adsorbed on both Bronsted- and Lewis-acid sites.[65,66] The distribution of acid sites (Lewis and Bronsted) on the various $AlPO_4$ catalysts is given in Table 3 as the amounts of PY and DMPY adsorbed at saturation at the given temperature. Thus, the site energy distribution was expressed in terms of the amount of base chemisorbed as a function of chemisorption temperature, which, in turn, is a measure of the strength or energy of the sites involved in chemisorption. As expected, the adsorption temperature determined the surface chemical interaction in all AlPO4 catalysts. As the temperature increased, surface acidity decreased because only the stronger acid sites were able to retain the probe molecule. Thus, adsorption capacities at 473 K accounted for total surface acidity (weak, medium, and strong acid sites) whereas those at 573 K were taken as an indication of relatively strong acid sites. The difference between PY and DMPY adsorption is one way to measure Lewis acid sites.

It is evident from Table 3 that the phosphate precursor scarcely affected the surface acidity of the final $AlPO_4$ catalyst; thus, for samples calcined at 773 and 923 K and independently of the phosphate precursor, there was no difference between the amounts of probe molecule adsorbed. Furthermore, the three $AlPO_4$ materials did not exhibit acidity when calcined at 1073−1273 K. In addition, the results in Table 3 also indicated that $AlPO_4$ catalysts obtained in the presence of an organic agent exhibited not only an increased total number of acid sites but also an increased number of strong acid sites (measured at 573 K) when compared to the AP-H3 catalyst. Even so, the specific organic agent along with the calcination temperature influenced the site energy distribution and the number of strong acid sites. Thus, for AP-ETD and AP-12PRD materials, surface acidity decreased as the calcination temperature rose to 1073 K; with a further increase in temperature surface acidity disappeared. For AP-13PRD and AP-24PED materials, however, surface acidity remained even after calcination at 1273 K. Moreover, calcination reduced not only the total number of acid sites capable of PY and DMPY adsorption but also their strength, causing a shift toward relatively weaker sites; although, Bronsted and Lewis acid sites coexisted on the AP-24PED-1273 surface. In addition, the number of strong acid sites in AP-24PED materials was higher than that in AP-13PRD ones.

Catalytic Activity. Cyclohexene skeletal isomerization (CSI) was studied as an acid-catalyzed reaction model to further characterize the acidic properties of $AlPO_4$ materials. In this respect, model reactions were recommended[68] as the best method for characterizing industrial catalysts. The advantage of applying test reactions for surface acidity characterization is that they were carried out under conditions similar to those that result from real catalytic reactions. There are several test reactions for solid acids[68,69] some of which are used for probing weakly acidic sites while others, e.g. hexane cracking, are suitable for very strongly acidic sites. CSI is one of the simplest reactions used to study relatively strong acid sites (Bronsted and Lewis) on solid catalysts.[68] In the conversion of cyclohexene, there were various possibilities: (i) skeletal isomerization to methylcyclopentene isomers; (ii) hydrogen transfer reaction to methylcyclopentane and cyclohexane; and (iii) dehydrogenation to benzene. In this sense, Parmaliana et

(64) Basolo, F.; Pearson, R. G. *Mechanisms of Inorganic Reactions*: *A Study of Metal Complexes in Solution*; Wiley: New York, 1968.
(65) Benesi, H. A. *J. Catal.* **1973**, *28*, 176.
(66) Corma, A.; Rodellas, C.; Fornes, V. *J. Catal.* **1984**, *88*, 374.
(67) Satsuma, A.; Kamiya, Y.; Westi, Y.; Hattori, T. *Appl. Catal. A* **2000**, *194−195*, 253.
(68) Guisnet, M. *Acc. Chem. Res.* **1990**, *23*, 392.
(69) Lercher, J. A.; Grundling, C.; Edel-Mirth, G. *Catal. Today* **1996**, *27*, 353.

Table 4. Apparent Rate Constants (K_a), Activation Parameters (E_a, ln A, $\Delta H^{\neq}$, and $\Delta S^{\neq}$) and Selectivities to 1-MCP (σ) for CSI on $AlPO_4$ Catalysts

catalyst	K_a 10^6 [a] (mol atm^{-1} g^{-1} s^{-1})	E_a (kcal mol^{-1})	ln A	$\Delta H^{\neq}$ (kcal mol^{-1})	$\Delta S^{\neq}$ (cal mol^{-1} K^{-1})	σ [b]
AP-H1-773	11.6	16.2	1.7	15.0	−58.3	1.3
AP-H1-923	10.1	18.2	3.2	16.9	−55.4	1.3
AP-H1-1073	0.2	*c*	*c*	*c*	*c*	*d*
AP-H2-773	9.9	15.0	0.6	13.8	−60.5	1.3
AP-H2-923	9.8	17.1	2.3	15.8	−57.3	1.3
AP-H2-1073	0.2	*c*	*c*	*c*	*c*	*d*
AP-H3-773	12.0	15.3	1.0	14.1	−59.7	1.3
AP-H3-923	12.2	16.0	1.6	14.7	−58.5	1.3
AP-H3-1073	0.3	*c*	*c*	*c*	*c*	*d*
AP-ETD-773	13.2	15.8	1.6	14.6	−58.5	1.3
AP-ETD-923	10.6	16.2	1.7	15.0	−58.4	1.2
AP-ETD-1073	7.1	19.3	3.8	18.1	−54.3	1.1
AP-ETD-1273	*e*					
AP-12PRD-773	12.2	16.4	1.9	15.2	−57.8	1.4
AP-12PRD-923	11.1	16.3	1.8	15.1	−57.9	1.1
AP-12PRD-1073	10.8	16.9	2.4	15.6	−56.8	1.1
AP-12PRD-1273	*e*					
AP-13PRD-773	14.4	15.7	1.5	14.5	−58.6	1.4
AP-13PRD-923	10.4	16.7	2.0	15.5	−57.6	1.2
AP-13PRD-1073	10.1	15.4	1.0	14.1	−59.6	1.1
AP-13PRD-1273	2.6	16.8	0.7	15.5	−60.2	1.0
AP-24PED-773	15.2	14.4	0.5	13.2	−60.6	1.5
AP-24PED-923	11.1	15.2	0.8	14.0	−59.9	1.2
AP-24PED-1073	11.4	15.4	1.0	14.2	−59.7	1.2
AP-24PED-1273	9.8	15.8	0.6	14.5	−60.6	1.1

[a] At a reaction temperature of 623 K. [b] Ratio of the fractional conversion of 1-MCMPE to 3-MCP. [c] Not measured. [d] Only 1-MCP. [e] No reaction.

al.[70] indicated that cyclohexene could be considered a most reliable probe molecule for a number of catalytic functions such as isomerization, hydrogen activation, and hydrogen transfer. So, the extent of these reactions in different samples provided a way of measuring strong-acid center concentrations.

The results of this study indicated that cyclohexene conversion proceeded simply by skeletal isomerization to 1- and 3-methylcyclopentene on all $AlPO_4$ catalysts. Moreover, in the absence of external and internal diffusional influences, the conversion reaction data (below 20%, where the equilibrium reaction can be ignored) were found to fulfill the Bassett−Habgood rate equation[71] for first-order reactions when the partial reactant pressure is low and the adsorption rate is faster than the rate of surface reaction, which is the rate-determining step. The Bassett−Habgood equation was in the form

$$\ln [1/(1 - X)] = k_a RT (W/F)$$

where X is cyclohexene conversion, k_a is the apparent rate constant of the surface process, W is the catalyst weight, and F is the flow rate of the carrier gas. Table 4 gives, for all $AlPO_4$ catalysts, apparent rate constants (k_a, at a reaction temperature of 623 K), from linear plots of ln $[1/(1 - X)]$ vs F^{-1}. Table 4 also includes activation parameters (E_a, ln A, $\Delta H^{\neq}$, and $\Delta S^{\neq}$), obtained from the Arrhenius and Eyring equations by plotting, respectively, ln k_a vs T^{-1} and ln kK/T vs T^{-1}. The kinetic selectivity factors (σ),[72] obtained from the slope of X_{1MCP} vs X_{3MCP} plots, are also included in Table 4. The 98% confidence limits and the determination coefficient (always over 0.99) for regressions were used to check the adequacy of the data. A Student's t test of significance showed that these were significant at levels over 1%. Moreover, at least three measurements were used to calculate each k_a value, and these were reproducible to within ca. 8%.

Strengthening acidity data, Table 4, showed that the phosphate precursor did not modify the catalytic performance of the final $AlPO_4$ catalyst and that for calcination temperatures over 923 K, the activity disappeared completely. This fact is due to $AlPO_4$ crystallization (see above). It is also evident from Table 4 that the presence of an organic agent developed $AlPO_4$ catalysts that exhibited increased activity in CSI as compared to AP-H3, especially at a treatment temperature of 1073/1273 K, where AP-H3 is practically inactive. Moreover, the decrease in catalytic activity on calcining at 1073/1273 K depended on the organic agent used. Thus, it should be noted that after calcining at 1273 K, the cyclohexene conversion levels of AP-24PED were higher (ca. 4 times) than those obtained for AP-13PRD, whereas AP-12PRD-1273 and AP-ETD-1273 were inactive. This fact corresponded to the high surface acidity of AP-24PED-1073/1273 catalyst in relation to the remaining ones. This was due to the strong inhibition of $AlPO_4$ crystallization by the presence of the 2-methyl-2,4-pentanediol. Furthermore, the change in activity with the change in both organic agent and calcination temperature was similar to the change in acidic characteristics shown in Table 3. So, the catalytic activity of $AlPO_4$ catalysts correlated well with the surface acidity measured gas-chromatographically through PY and DMPY adsorption. The pretreatment effect can be understood in terms of the dehydroxylation of the surface that converted Bronsted acid sites into Lewis acid sites. Such a conversion lowered the

(70) Parmaliana, A.; Iannibello, A.; Frusteri, F.; Tsiakaras, T.; Giordano, N. *Catalysis 1987*; Elsevier: New York, 1988; p 43.
(71) Bassett, D.; Habgood, H. W. *J. Phys. Chem.* **1960**, *64*, 769.
(72) Wheeler, A. *Adv. Catal.* **1951**, *3*, 529.

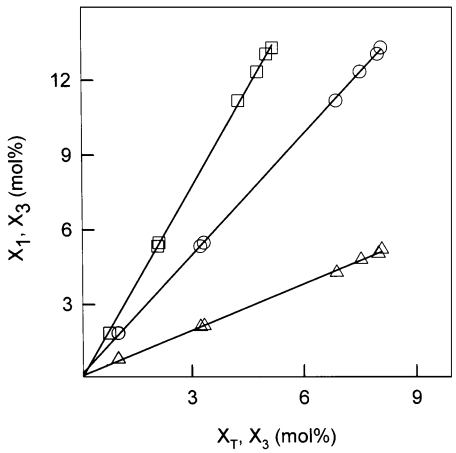

Figure 11. OPE selectivity curves [(○) X_1 and (△) X_3 vs X_T] and Wheeler selectivity [σ; (□) X_1 vs X_3] for cyclohexene skeletal isomerization on AP-24PED-773 catalyst.

concentration of Bronsted acid sites and, in turn, CSI activity.

Selectivity Studies. With regard to the selectivity of the CSI reaction, we have constructed the optimum performance envelope (OPE) curves which describe the selectivity behavior of products, as described by Ko and Wojciechowski.[73] The OPE curves represent the conventional selectivity behavior of the active sites present on a fresh catalyst and whose slope at the origin represents the initial selectivity for that product. The curves were obtained by plotting the fractional conversion to 1-MCP (X_1) or 3-MCP (X_3), against total conversion (X_T) for different weight ratios of catalyst to the cyclohexene introduced. OPE curves for AP-24PED-773 catalyst appear in Figure 11. We have plotted all the experimental data corresponding to different reaction temperatures and contact times on the same diagram (the overall conversion was always below 20 mol %). Using such a procedure, an insignificant scattering of the data was evident on the selectivity diagrams and so clear tendencies can be observed from these plots. The results (straight lines at origin in all cases) showed that, in the range of conversions studied, 1- and 3-MCP were stable primary competitive products coming from cyclohexene through a parallel process with first-order kinetics. They were formed at a constant rate in relation to feed conversion and neither disappeared nor accumulated due to secondary products. A primary product was defined as that produced from the reactant, no matter how many surface intermediates are involved in its formation. Besides, these isomerization products were really competitors, with first-order kinetics, as straight lines are obtained from the application of the Wheeler criterion[72] (X_1 vs X_3 plots, Figure 11) on the kinetic selectivity factor (σ). Thus, for a parallel process when a first-order kinetics is followed, σ can be written as

$$\sigma = k_1/k_3 = X_1/X_3$$

As Figure 11 contains points at all reaction temperatures, the activation energies for 1- and 3-MCP formation were identical for each catalyst (as to be expected for a mechanism involving a carbenium ion intermediate) and so they were formed on the same active sites. Both this and the fact that the apparent activation energy for CSI does not vary from catalyst to catalyst within the limits of our experimental error let us assume that the variations in catalytic activity observed in the different catalysts under consideration were therefore due to variations in the number and strength of active acid sites rather than differences in the nature of the active sites or a change in the mechanism. Thus, as in previous studies[2,16] different σ values were due to the different A_1/A_3 ratios according to

$$\sigma = k_1/k_3 = X_1/X_3 = [A_1 \exp(-E_{a1}/RT)]/[A_3 \exp(-E_{a3}/RT)] = A_1/A_3$$

Thus, as the preexponential factor is a function of strong acid site number and this was different on each catalyst, the σ values are also different.

On the other hand, there was a relationship between the values of $\Delta H^{\neq}$ and $\Delta S^{\neq}$ (as well as between ln A and E_a) as shown in the expression for the compensation effect or isokinetic relationship.[74−77]

$$\Delta G^{\neq} = -\theta R \ln K^{\neq} = \Delta H^{\neq} - \theta \Delta S^{\neq}$$

where R is the gas constant, $K^{\neq}$ is the equilibrium constant of the activated complex, and θ is the isokinetic temperature. In fact, although some points are scattered, the plot of $\Delta H^{\neq}$ vs $\Delta S^{\neq}$ (or ln A vs E_a) for the CSI reaction process indicates a reasonable linear correlation (with regression coefficients over 0.96) for all catalysts. θ and $K^{\neq}$ were obtained from the slope and intercept. When a compensation effect holds for a reaction occurring on a series of homologous catalysts, a single common interaction mechanism and, consequently, a common transition-state intermediate, can be expected for all catalysts.[74−77]

The effect is interpreted essentially as a consequence of the heterogeneity of acidic sites[77] due to the fact that the catalytic reaction involves adsorbed species and that the surface heterogeneity of the catalysts affects the activation energy (or $\Delta H^{\neq}$) for the reaction. Thus, the distribution of acid strength determines the energy barrier for the reaction to occur; the number of sites is important also. So, the global rate will be the sum of the individual rates on each type of acid site, each one proceeding from different activation energy ($\Delta H^{\neq}$). The differences in reaction rate originate in changes in the energetics and number of reactive species. Moreover, the number of sites active for a given reaction depends mainly on the activation energy.[74] Thus, strong acid sites are characterized by lower activation energy (or $\Delta H^{\neq}$) while the relative abundance of such sites can be related to their relative activity. So, those catalytic materials with higher acidity, which correspond to a lower activation energy, should have a lower density of acid sites.

(73) Ko, A. N.; Wojciechowski, B. W. *Prog. React. Kinet.* **1983**, *12*, 201.
(74) Maatman, R. W. *Adv. Catal.* **1980**, *9*, 51.
(75) Curtis-Conner, W., Jr. *J. Catal.* **1982**, *78*, 238.
(76) Linert, W.; Soukup, R. W.; Schmid, R. *Comput. Chem.* **1982**, *6*, 47.
(77) Corma, A.; Lopis, F.; Monton, J. B.; Weller, S. *J. Catal.* **1993**, *142*, 97.

One could explain the compensation effect on this series of $AlPO_4$ catalysts by considering that if a range of acid sites with different acid strength were present, each one of them would need a different activation enthalpy (or E_a) to carry out the reaction. As a rule, it can be expected that the stronger the acidity, the lower the increase of enthalpy between the reactants and the activated complex, and also the lower the entropy of such a complex. Then going from one $AlPO_4$ catalyst to another, one does not expect it to be the nature of the active sites that changes but rather the acid strength distribution, and, consequently, the resultant "averaged" activation enthalpy observed experimentally. So, the differences between the activities of $AlPO_4$ materials were due to differences in the number and strength of acid sites. The balance between (i) the amount of acid sites, which affected mainly the frequency factor values, and (ii) their activity, which affected mainly the activation energy, determined the sequence of catalytic activity in $AlPO_4$ catalysts.

Conclusions

The presence of a dihydroxylated organic additive in the synthesis medium considerably influenced the surface properties of $AlPO_4$ catalysts. The results indicated that $AlPO_4$ catalysts, when prepared by a gel precipitation method in the presence of a dihydroxylated organic agent, exhibited higher thermal stability and retained larger surface areas (up to 40 times higher) and pore volumes (with a small increase in pore diameter) than $AlPO_4$ prepared without this type of organic agent. Furthermore, these catalysts remained in the amorphous state at calcination temperatures up to 1073 K. Thermal treatment at 1273 K developed α-cristobalite crystalline $AlPO_4$ materials (with very low surface areas) when 1,2-ethanediol or 1,2-propanediol were used, although in the case of 1,3-propanediol and, especially, with 2-methyl-2,4-pentanediol, $AlPO_4$ catalysts still retained a mesoporous structure with a relatively large surface area. Furthermore, they exhibited a higher number of Bronsted acid sites as well as an improved catalytic performance for the cyclohexene skeletal isomerization process. Moreover, catalytic activity resulting in CSI reaction can be well interpreted in terms of differences in the number and strength of acid sites which are measured gas chromatographically in terms of pyridine and 2,6-dimethylpyridine adsorbed at 473 and 573 K. The hydrophilic character, the number of hydrophobic groups, and the steric hindrance of dihydroxylated organic molecules play an important role in the amorphous $AlPO_4$ forming process. Thus, the use of an organic agent that can interact with aluminum ions proves to be effective for the preparation of $AlPO_4$ materials with higher thermal stabilities and results in more stable porous texture exhibiting large surface areas, pore volumes, and surface acidities, even after calcination at 1073−1273 K.

Acknowledgment. The present work was subsidized by grants from the Dirección General de Investigación (Project BQU-2001-2605, Ministerio de Ciencia y Tecnología), FEDER funds, and from the Consejería de Educación y Ciencia (Junta de Andalucía). We thank Professor M. Sullivan for linguistic revision of the manuscript.

CM030206+